MATERIALS CHEMISTRY
FRONTIERS

RESEARCH ARTICLE

View Article Online
View Journal | View Issue

Cite this: *Mater. Chem. Front.*, 2018, **2**, 338

Sterically crowded hydrogen-bonded hexagonal network frameworks†

Ichiro Hisaki,*[a] Nobuaki Ikenaka,[a] Seiji Tsuzuki[b] and Norimitsu Tohnai[a]

Received 29th November 2017,
Accepted 7th December 2017

DOI: 10.1039/c7qm00544j

rsc.li/frontiers-materials

A hydrogen-bonded hexagonal network (H-HexNet) composed of C_3-symmetric π-conjugated molecules with six carboxyphenyl groups is one of the candidate platforms for porous organic materials. For formation of H-HexNets, a triangular cyclic structure, a so-called phenylene triangle (PhT) motif, composed of hydrogen bonded carboxyphenyl groups is a key structure. In this paper, we synthesized two derivatives of hexakis(carboxyphenyl)triphenylene **TpMe** and **TpF**, in which substituents (Me or F) were introduced in the *ortho*-positions of the carboxy groups, to investigate whether the PhT motif forms and how the structure and property of H-HexNets are affected by steric bulkiness around the hydrogen bonding moieties. Crystal structures, thermal stability, evaluation of permanent porosity by gas sorption experiments, and photochemical properties are revealed, which can contribute to establishment and fine-tuning of porous organic materials based on H-HexNets.

Introduction

A hydrogen-bonded (H-bonded) dimer of carboxy groups is one of the simplest and the most well-known supramolecular synthons,[1] that is, structural units within supermolecules which can be formed and/or assembled by known or conceivable synthetic operations involving intermolecular interactions. The dimer, however, has been still an attractive H-bonding unit to achieve predesigned supramolecular architectures, due to its highly directional bonding nature and facile accessibility to a huge number of its derivatives.[2]

Two dimensionally networked porous frameworks based on organic molecules have been intensively investigated from the viewpoints of not only gas storage and separation,[3] catalysts[4] and sensors,[5] but also photoelectronic and (semi)conducting materials.[6] They include metal–organic frameworks (MOFs),[7] covalent organic frameworks (COFs),[8] and H-bonded organic frameworks (HOFs).[9] Introducing the carboxy groups into building block molecules with a well-defined geometry can yield such HOFs.[10] The pioneering system is the 2D honeycomb framework of trimesic acid, reported by March[10a] and Herbstein.[10b] Kobayashi also reported the layered assembly of a H-bonded hexagonal network (LA-H-HexNet) composed of hexakis(4-carboxyphenyl)benzene.[10c] Recently, some HOFs with permanent porosity have been constructed with carboxylic acid.[11] However, it is still challenging to establish a general way to access functional HOFs with tunable pore size, shape, and surface properties.

In connection with this, we have also demonstrated that a series of C_3-symmetric planar π-conjugated hydrocarbons, such as triphenylene (**Tp**), possessing three 4,4′-dicarboxy-*o*-terphenyl moieties in the periphery form a dual-pored HexNet through a cyclic H-bonded motif called a phenylene triangle (PhT) (Fig. 1c), and that the H-HexNet stacks without interpenetration to give layered HOFs (LA-H-HexNets) with porosity (Fig. 1a).[12]

The important structural feature of the building block is that the peripheral carboxy phenyl groups are not coplanar but twisted against the plane of the central core (Fig. 1d, left). This twisted conformation enhances the solubility of the molecules in common organic solvents, provides shape-persistent pores surrounded by rigid phenylene walls,[13] and plays a role in the stacking ways of H-HexNets to give layered structures.

In this study, we newly introduced substituents (Me or F) in the *ortho*-positions of the carboxy groups to force the carboxy and phenylene groups twisted (Fig. 1d, right), and investigated the effects of the substituents on molecular assemblies and properties. Regarding the steric effects of substituents on H-bonding, Ośmiałowsky demonstrated that bulkiness of substituents near the H-bonding moiety can both increase and decrease attractive interactions, depending on the situation.[14] Thus, understanding of sterical effects on H-bonding is essential for constructing molecular architectures. Furthermore, in the case of a fluorine substituted derivative, electrostatic repulsion between oxygen and fluorine atoms might also have an effect on molecular conformation and packing.[15]

[a] *Graduate School of Engineering, Osaka University, 2-1 Yamadaoka, Suita, Osaka 565-0871, Japan. E-mail: hisaki@mls.eng.osaka-u.ac.jp*
[b] *National Institute of Advanced Industrial Science and Technology (AIST), Tsukuba, Ibaraki 305-8568, Japan*

† Electronic supplementary information (ESI) available. CCDC 1578414–1578417. For ESI and crystallographic data in CIF or other electronic format see DOI: 10.1039/c7qm00544j

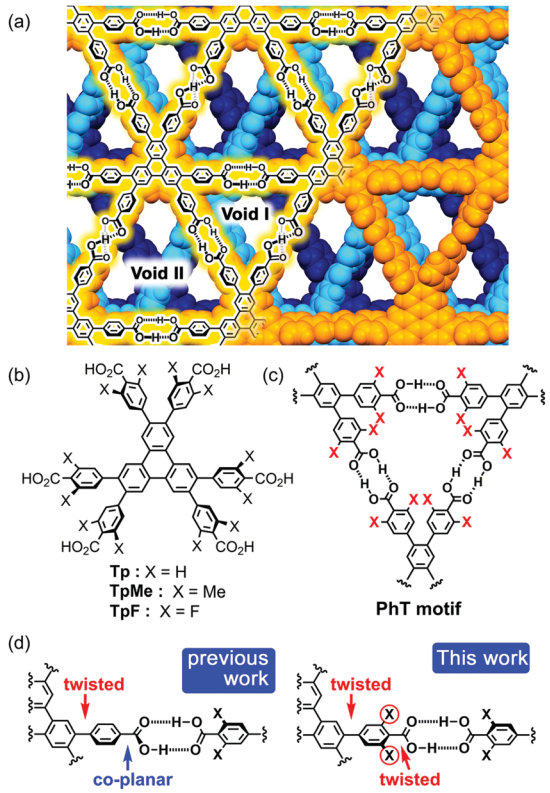

Fig. 1 (a) Layered assembly of hydrogen-bonded hexagonal network (LA-H-HexNet) structure composed of **Tp**. (b) Triphenylene derivatives **Tp**, **TpMe**, and **TpF**. (c) Hydrogen-bonded motif, so-called phenylene triangle (PhT) motif. (d) Twisted or co-planar conformation at the peripheral carboxyphenyl groups.

Herein, we describe the synthesis of hexakis(4-carboxy-3,5-dimethylphenyl)triphenylene **TpMe** and hexakis(4-carboxy-3,5-difluorophenyl)triphenylene **TpF** (Fig. 1b), crystal structures of their LA-H-HexNets, their thermal stability, evaluation of their permanent porosity by gas sorption experiments, and their photochemical properties. We revealed, for the first time, how the structure and property of H-HexNets are affected by sterically twisted conformation and bulkiness of the peripheral hydrogen bonding moieties.

Experimental

General

^{1}H and ^{13}C NMR spectra were measured using a Bruker (600 MHz for ^{1}H, 150 MHz for ^{13}C) or JEOL (400 MHz for ^{1}H, 376 MHz for ^{19}F) spectrometer. Residual ^{1}H and ^{13}C of the deuterated solvents were used as an internal standard [$CDCl_3$: 7.27 ppm and DMSO-d_6: 2.50 ppm for ^{1}H, $CDCl_3$: 77.00 ppm and DMSO-d_6: 39.51 ppm for ^{13}C]. For ^{19}F NMR, 0.05%-$C_6H_5CF_3$ in C_6D_6 was used as an external standard (−62.0 ppm). Mass spectrum data were obtained from a JEOL JMS-700 instrument or Autoflex III Bruker. FT-IR spectra of the synthesized compounds were recorded using a JASCO FT/IR-4200 spectrometer. Thermogravimetric (TG) and differential thermal (DT) analyses were performed using a Thermo Plus 8120 (Rigaku) instrument under N_2 purge at a heating rate of 5 °C min^{-1}. Emission and excitation spectra in solid states were measured using a JASCO FP-6500 spectrofluorometer. Powder X-ray diffraction (PXRD) data were collected on a Rigaku Ultima-IV using graphite-monochromatized Cu-Kα radiation (λ = 1.54187 Å) at room temperature. Gas sorption measurements were performed on BELSORP-max.

Single crystal X-ray analysis

For crystals **TpMe-1**, **TpMe-3**, and **TpF-1**, diffraction data were collected on a two-dimensional X-ray detector (PILATUS 200K/R) equipped in a Rigaku XtaLAB P200 diffractometer using multi-layer mirror monochromated Cu-Kα radiation (λ = 1.54187 Å). The cell refinements were performed with the software CrysAlisPro 1.171.38.41o.[16] For crystals **TpMe-2**, diffraction data were collected on a CCD (MX225HE, Rayonix) with synchrotron radiation (λ = 0.8000 Å) monochromated by the fixed exit Si (111) double crystal. The cell refinements were performed with HKL2000 software.[17] Direct methods (SHELXT)[18] were used for the structure solution of the crystals. All calculations were

Table 1 Crystal data of **TpMe-1**, **TpMe-2**, **TpMe-3**, and **TpF-1**

	TpMe-1	**TpMe-2**	**TpMe-3**	**TpF-1**
Formula	$C_{72}H_{60}O_{12}\cdot\cdot\cdot C_8H_8O_2$	$C_{72}H_{60}O_{12}$	$C_{72}H_{60}O_{12}$	$C_{60}H_{24}F_{12}O_{12}$
FW	1253.41	1117.26	1117.26	1164.82
Crystal system	Monoclinic	Triclinic	Triclinic	Monoclinic
Space group	*I*2/*a*	*P*$\bar{1}$	*P*$\bar{1}$	*I*2/*a*
a [Å]	27.8455(3)	13.2528(3)	14.5930(5)	12.2591(3)
b [Å]	22.4501(2)	16.2730(4)	15.3214(5)	38.9347(8)
c [Å]	29.8331(3)	18.7976(4)	20.3750(6)	18.0305(4)
α [°]	90	100.6586(8)	102.970(2)	90
β [°]	95.3352(9)	93.1880(8)	102.468(3)	93.869(2)
γ [°]	90	98.3918(14)	97.238(3)	90
V [Å^3]	18568.9(3)	3927.09(16)	4261.2(3)	8586.4(3)
Z/*Z*′	4/1	2/1	2/1	2/1
R_1 [$I < 2\sigma(I)$]	0.0883	0.1263	0.1052	0.1062
R_w (all)	0.2926	0.4165	0.3608	0.3799
Obs./unique reflns.	54132/18891	20624/10145	40581/17192	41187/8961
T/K	213	213	213	213
CCDC	1578416	1578414	1578415	1578417

performed with the observed reflections [$I > 2\sigma(I)$] with the program CrystalStructure crystallographic software packages,[19] except for refinement which was performed by SHELXL.[20] All non-hydrogen atoms were refined with anisotropic displacement parameters, and hydrogen atoms were placed in idealized positions and refined as rigid atoms with the relative isotropic displacement parameters. The SQUEEZE function equipped in the PLATON program was used to remove disordered solvent molecules in voids.[21] Crystal data are listed in Table 1.

Variable temperature (VT) PXRD measurements

The crystalline bulk placed on an aluminum substrate was subjected to VT-PXRD measurements under the air atmosphere. PXRD data were collected on a Rigaku Ultima-IV using graphite-monochromatized Cu-Kα radiation (λ = 1.54187 Å). The temperature of the sample was increased from room temperature to 360 °C at a rate of 1 °C min^{-1}. During the temperature increase, XRD patterns ranging from 3° to 18° were repeatedly recorded with a scan rate of 3° min^{-1}. Therefore, one PXRD scan has a temperature width of 5 °C.

Ab initio calculations

The geometries of **1-H**, **1-Me**, and **1-F** (Chart 1) and their hydrogen bonded dimers were optimized at the MP2/6-311G** level using the Gaussian 09 program.[22] Vibration analysis showed that the optimized structures are energy minimum structures. Conformational energies were calculated at the MP2/6-311G** level. The intermolecular interaction energies (E_{int}) were calculated at the MP2/cc-pVTZ level by the supermolecule method. The basis set superposition error (BSSE)[23] was corrected for all the interaction energy calculations using the counterpoise method.[24] The stabilization energy for forming a dimer from the isolated monomers (E_{form}) was calculated as the sum of E_{int} and the deformation energy (E_{def}), which is the sum of the increase in energy due to the deformation of the monomers during formation of the dimer. Here, E_{def} was calculated at the MP2/cc-pVTZ level.

Synthesis

Hexakis(4-methoxycarbonyl-3,5-dimethylphenyl)triphenylene derivative 4. A mixture of 2,3,6,7,10,11-hexabromotriphenyelene (1.00 g, 1.43 mmol), 3,5-dimethyl-4-methoxycarbonylphenylboronic acid **2** (2.12 g, 10.2 mmol), Pd(dppf)Cl_2 (0.938 g, 1.28 mmol) and K_2CO_3 (2.36 g, 17.1 mmol) in deoxygenated toluene (100 mL), 1,4-dioxane (50 mL), and methanol (50 mL) was stirred for 72 h under reflux conditions. The reaction mixture was extracted with $CHCl_3$, washed with water and brine, and dried over anhydrous $MgSO_4$. The product was purified by column chromatography (silica gel, $CHCl_3$: hexane = 5 : 1) to give **4** (1.08 g, 0.915 mmol, 64%) as a pale yellow solid. M.p.: 338 °C (decomp.). ^{1}H NMR (600 MHz, $CDCl_3$): δ 8.62 (s, 6H), 7.02 (s, 12H), 3.94 (s, 18H), 2.30 (s, 36H) ppm. ^{13}C NMR (150 MHz, $CDCl_3$): δ 19.87, 51.90, 125.50, 128.94, 129.23, 132.41, 135.08, 139.32, 142.24, 170.37 ppm. FT-IR (KBr): ν = 2947, 1717, 1606, 1570, 1502, 1437, 1378, 1266, 1190, 1115, 1093, 1078, 870, 822, 802, 784, 754, 732, 681 cm^{-1}. HR-MS (FAB): *m*/*z* calc. for $[M]^+$ $C_{78}H_{72}O_{12}$ 1200.502; measured 1200.502.

TpMe. Methyl ester derivative **4** (1.40 g, 1.17 mmol) in trifluoroacetic acid (140 mL) and water (5 mL) was stirred for 96 h under reflux conditions. The precipitate was filtered and washed with $CHCl_3$. The product was dissolved in acetone, followed by the addition of hexane, yielding pure **TpMe** (0.837 g, 0.749 mmol, 64%) as a pale yellow solid. M.p.: 310 °C (decomp.). ^{1}H NMR (600 MHz, DMSO-d_6): δ 8.80 (s, 6H), 7.06 (s, 12H), 2.22 (s, 36H) ppm. ^{13}C NMR (150 MHz, DMSO-d_6): δ 170.72, 140.98, 139.39, 133.85, 133.23, 129.00, 128.33, 125.40, 19.37 ppm. FT-IR (KBr): ν = 3648, 2926, 2366, 1712, 1604, 1500, 1435, 1381, 1274, 1123, 1077, 1035, 872, 803, 735 cm^{-1}. HR-MS (MALDI): *m*/*z* calc. for $[M - H]^-$ $C_{72}H_{59}O_{12}$ 1115.408; measured 1115.623.

Hexakis(4-methoxycarbonyl-3,5-difluorophenyl)triphenylene derivative 5. A mixture of 2,3,6,7,10,11-hexabromotriphenylene (52.6 mg, 75.0 μmol), 3,5-difluoro-4-methoxycarbonylphenylboronic acid pinacolyl ester **3** (166 mg, 0.551 mmol), $PdCl_2$(dppf) (31.3 mg, 43.1 μmol), and Na_2CO_3 (81.5 mg, 0.769 mmol) in deoxygenated toluene (10 mL), 1,4-dioxane (5.0 mL), and methanol (5.0 mL) was stirred for 40 h under reflux conditions. The reaction mixture was extracted with $CHCl_3$, washed with water and brine, and dried over anhydrous $MgSO_4$. The product was purified by column chromatography (silica gel, $CHCl_3$: AcOEt = 50 : 1) to give **5** (34.6 mg, 27.8 μmol, 34%) as a pale yellow solid. M.p.: 264 °C (decomp.). ^{1}H NMR (400 MHz, $CDCl_3$): δ 8.64 (s, 6H), 6.96 (d, 12H, J = 8.4 Hz), 3.99 (s, 18H) ppm. ^{13}C NMR (150 MHz, $CDCl_3$): δ 161.50, 159.82, 145.08, 137.59, 129.55, 125.93, 113.58, 110.22, 52.90 ppm. ^{19}F NMR (367 MHz, $CDCl_3$): δ −107.73, −107.75 ppm. FT-IR (KBr): ν = 2360, 1735, 1636, 1560, 1434, 1402, 1329, 1274, 1192, 1107, 1069, 1042, 884, 863, 827, 788, 592, 530 cm^{-1}. HR-MS (FAB): *m*/*z* calc. for $[M]^+$ $C_{66}H_{48}F_{12}O_{12}$ 1248.202; measured 1248.202.

TpF. Methyl ester derivative **5** (33.2 mg, 26.5 μmol) in THF (10 mL) and 2% KOH aqueous solution (5.0 mL) was stirred for 40 h at 50 °C. THF was evaporated *in vacuo* and the resultant aqueous solution was filtered. To the filtrate, 12 M HCl was added dropwise until the solution became acidic. The precipitate was filtered, washed with water, and dried *in vacuo*, to yield **TpF** (26.5 mg, 22.5 μmol, 85%) as a pale brown solid. M.p. 214 °C (decomp.). ^{1}H NMR (600 MHz, DMSO-d_6): δ 9.12 (s, 6H), 7.27 (d, 12H, J = 9.2 Hz) ppm. ^{13}C NMR (150 MHz, DMSO-d_6): δ 162.06, 159.68, 158.01, 144.61, 137.20, 129.20, 126.52, 114.25 ppm. ^{19}F NMR (367 MHz, DMSO-d_6): δ −111.6, −111.63 ppm. FT-IR (KBr): ν = 2925, 2360, 1701, 1636, 1560, 1430, 1278, 1124, 1043, 864, 807, 576 cm^{-1}. HR-MS (MALDI): *m*/*z* calc. for $[M]^-$ $C_{60}H_{24}F_{12}O_{12}$ 1164.108; measured 1664.015.

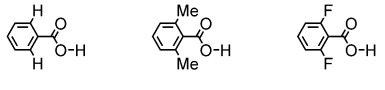

1-H 1-Me 1-F

Chart 1 Model compounds for calculation.

Results and discussion

Theoretical calculation of hydrogen bonding

To investigate the *ortho*-substitution effects on the structures and magnitude of the interactions of the hydrogen bonded dimer,

Table 2 Stabilization energy of dimers (kcal mol^{-1})

Dimer	E_{int}[a]	E_{def}[b]	E_{form}[c]
1-H	−18.0	2.5	−15.4
1-F	−17.1	2.3	−14.8
1-Me	−17.7	2.5	−15.2

[a] E_{int} is the intermolecular interaction energy calculated for the hydrogen bonded dimer at the MP2/cc-pVTZ level. [b] E_{def} is the deformation energy. [c] E_{form} is the stabilization energy for the formation of a dimer, which is the sum of E_{int} and E_{def}. See text for details.

three model systems **1-H**, **1-Me**, and **1-F** were subjected to theoretical calculation (Chart 1). In contrast to **1-H**, which has a coplanar conformation (ω = 0°, where ω denotes dihedral angles between the benzene ring and the carboxy group), **1-Me** and **1-F** have a twisted conformation (ω = 53.8° and 54.5°, respectively) due to steric hindrance of the substituents. The co-planar conformers of **1-Me** and **1-F** are less stable than the corresponding twisted energy minimum conformers by as much as 2.37 kcal mol^{-1} and 1.86 kcal mol^{-1}, respectively. The **1-Me** and **1-F** dimers have two nearly isoenergetic isomers shown in Fig. S1 (ESI†). The energy differences between the isomers are less than 0.1 kcal mol^{-1}.

Subsequently, the E_{form} for the dimers of **1-H**, **1-Me**, and **1-F** was calculated (Table 2). Stabilization energies of the dimers of **1-H**, **1-Me**, and **1-F** range from −14.8 to −15.4 kcal mol^{-1}, indicating that substituent effects on hydrogen bonding energy are negligible. This result is consistent with the atomic charges on carbonyl oxygen atoms and hydrogen atoms of the carboxy group in **1-H**, **1-Me** and **1-F** obtained by *ab initio* calculations (Table S2, ESI†). The charges on these atoms are nearly identical in the three molecules, in spite of the different *o*-substituents. To further elucidate the substituent effects on the hydrogen bonds of the carboxy group, we evaluated the interactions of carboxylic acids (**1-H**, **1-Me**, **1-F**) with Na^+ and Cl^- as shown in Fig. S2 and S3 (ESI†). No significant differences were observed among the interactions of these three carboxylic acids with Na^+ and Cl^-.

Synthesis and crystallization of TpMe and TpF

Hexakis(methoxycarbonylphenyl)triphenylene derivatives **4** and **5** were synthesized in 64% and 37%, respectively, by Suzuki–Miyaura cross coupling of 2,3,6,7,10,11-hexabromotriphenylene and the corresponding boronic acid **2** or pinacol borate **3** in the presence of Pd(dppf)Cl_2 and bases. Subsequently, hydrolysis of **4** and **5** was performed with CF_3CO_2H and KOH, respectively, to yield **TpMe** and **TpF** in 64% and 85% yields, respectively (Scheme 1a).

TpMe and **TpF** were recrystallized by slow evaporation of a mixed solution of DMF and methyl benzoate at 50 °C to yield single crystals suitable for X-ray crystallographic analysis (Scheme 1b). **TpMe** yielded totally three polymorphic crystals **TpMe-1**, **TpMe-2**, and **TpMe-3** under the same conditions. However, it needs to be mentioned that it is not clear whether three polymorphs are always contained in the crystalline bulk formed in the same batch, because a general diffractometer in the laboratory provided only weak and ambiguous XRD patterns for the obtained crystalline materials due to the low electron

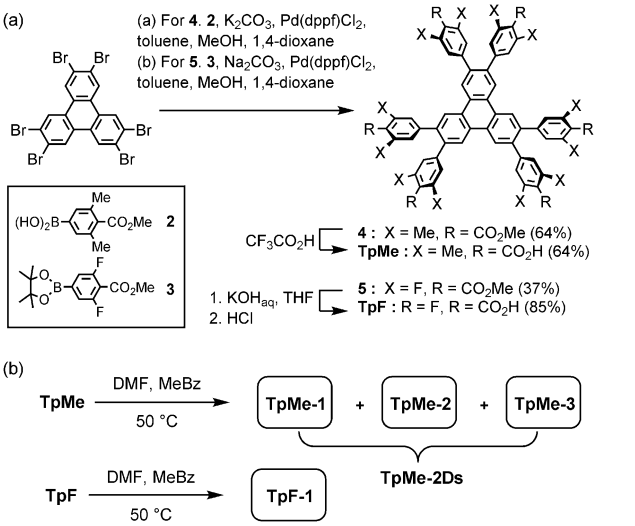

Scheme 1 (a) Synthesis and (b) crystallization of hexasubstituted triphenylene derivatives **TpMe** and **TpF**. Abbreviations, DMF: *N*,*N*-dimethylformamide, MeBz: methyl benzoate.

density contrast generated by disordered methyl benzoate molecules within the pores, making it difficult to characterize the polymorphic forms. Therefore, such bulk crystals obtained by crystallization at 50 °C are called **TpMe-2Ds.** On the other hand, **TpF** yielded one crystalline form **TpF-1**.

Crystal structures of HexNet frameworks

In the crystal structures of **TpMe-1**, **TpMe-2**, and **TpMe-3** (Fig. 2), **TpMe** forms a H-HexNet, which stacks in a non-interpenetrated manner to give layered assemblies (LA-H-HexNets). **TpMe-1** shows conformational disorder at five carboxy groups due to steric hindrance of the *o*-substituents as shown by yellow atoms in Fig. 2a. This kind of rotational disorder was expected, as predicted by the theoretical calculation. However, to our surprise, the other polymorphs show no rotational disorder at the carboxy groups, and furthermore, all three polymorphs have no disorder at the phenylene groups, although their anisotropic displacement ellipsoids are more extended compared with those of the triphenylene core. The void ratios in **TpMe-1**, **TpMe-2**, and **TpMe-3** are 45.2%, 35.9%, and 41.5%, respectively, which are relatively small compared with LA-H-HexNets of **Tp** (50.0–54.4%) due to the bulky substituents.[12b] In the void spaces, methyl benzoate molecules are accommodated, although they are severely disordered.

The present polymorphs were caused by versatile conformations of the phenylene groups and slightly different stacking manners of the HexNet sheets. To evaluate the conformational versatility of the peripheral carboxy phenyl moieties, the following two parameters ϕ and ω were introduced (Fig. 3), where ϕ denotes the dihedral angle between the triphenylene core and the phenylene ring and ω denotes the dihedral angle between the phenylene ring and the carboxy group. The values are listed in Table 3. As we expected, dihedral angle ϕ in the **TpMe** polymorphs ranges from −75.8° to +55.7°, which is similar to that of **Tp-1**. On the other hand, dihedral angle ω in the **TpMe**

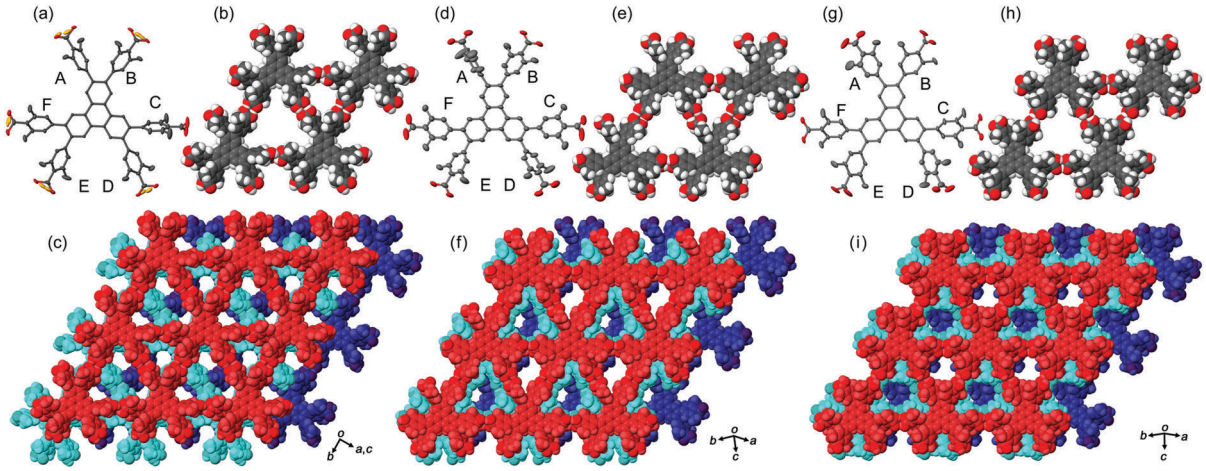

Fig. 2 Crystal structures of (a–c) **TpMe-1**, (d–f) **TpMe-2**, and (g–i) **TpMe-3**. (a, d and g) Molecular conformation drawn in anisotropic displacement ellipsoids with 50% probability. (d, e and h) Motif of HexNet frameworks. (c, f and i) Layered packing diagram composed of three HexNet sheets. Void spaces are filled by methyl benzoate used as a solvent, although most of them cannot be solved crystallographically due to severe disorder.

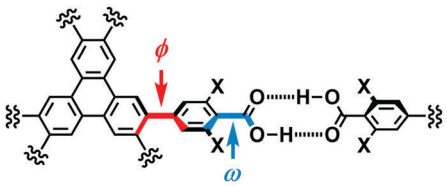

Fig. 3 Definition of two parameters related to conformations of the phenylene and carboxy groups: dihedral angles ϕ and ω, respectively.

Table 3 Values of ϕ and ω in three polymorphs of **TpMe**, **TpF-1**, and the previously reported pristine system **Tp-1**

ϕ	TpMe-1	TpMe-2	TpMe-3	TpF-1[a]	Tp-1[b]
A	+55.7	−75.8	+49.8	+59, −59	+52.7
B	+44.0	−50.0	+40.1	+59, −59	+52.4*[c]
C	−62.4	−32.5	+48.8	−58, +62	−49.6
D	−47.4	−65.6	+47.7	−59, +52	−46.6
E	−49.0	+54.5	−40.0	−59, +52	+67.4*[c]
F	−46.7	+32.0	−54.7	−58, +62	+52.8
Conf.[d]	PMM	MMP	PPM	—	PMP

ω	TpMe-1[e]	TpMe-2	TpMe-3	TpF-1[f]	Tp-1
A	−62.8	+71.4	−52.5	30–90	−4.3
B	−63.4	+46.9	−87.0	30–90	11.3*[c]
C	−46.9	+68.0	−41.7	20–30	3.0
D	−54.9	+68.6	+80.4	20–90	4.4
E	+63.7	−48.2	+84.9	20–90	11.5*[c]
F	+41.6	−66.0	+42.1	20–30	2.7

[a] Two kinds of values are described due to the disorder of the phenylene groups. [b] Ref. 12*b*. [c] An asterisk (*) denotes that the conformational frustration is located in the corresponding peripheral group. [d] Classification of the conformers; for details, see ref. 12*b*. [e] For **TpMe-1**, only major conformation is applied to show the ω value. [f] Approximated range of torsion angles are listed due to highly elongated anisotropic displacement parameters.

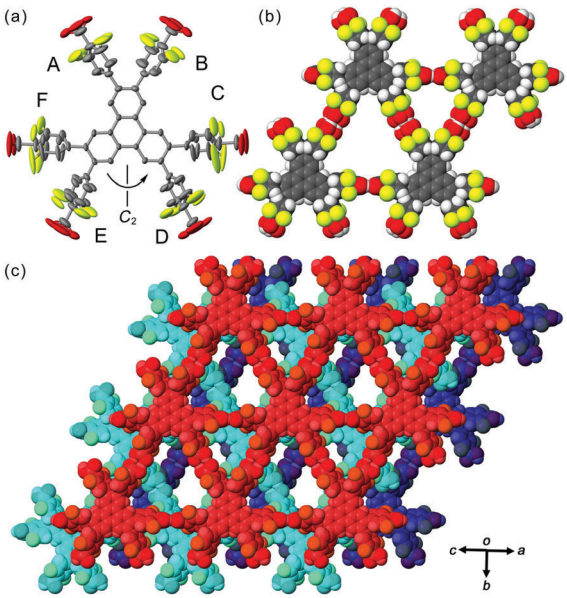

Fig. 4 Crystal structure of **TpF-1**. (a) Molecular structure with anisotropic displacement ellipsoid with 50% probability, where the peripheral carboxy and difluorophenylene groups are severely disordered. (b) Rhombic motif. (c) Layered framework composed of three HexNet sheets, in which one of the disordered structures was applied for clarity.

polymorphs ranges from −87.0° to +84.9°, which is significantly larger compared to that of **Tp-1** (*i.e.* −4.3° to +11.5°).[12b]

In contrast to **TpMe**, **TpF** has yielded one crystalline form **TpF-1** under the same crystallization conditions as with **TpMe** (Fig. 4). In the crystal structure, the **TpF** molecule with a two-fold axis forms a LA-H-HexNet with a stacking manner similar to that of **TpMe-1**. The void ratio of **TpF-1** is 50.4% and severely disordered methyl benzoate molecules are accommodated in the void. Interestingly, all the phenylene groups and four of six carboxy groups are rotationally disordered into two positions and their anisotropic displacement ellipsoids are also elongated. The phenylene rings of the molecule in **TpF-1** are twisted as observed in other **TpMe** and **Tp-1** systems (see ϕ values in Table 3). The carboxy groups are also twisted against the plane of the phenylene rings: ω values range from 20° to 90°,

although the exact values are not presented due to the relatively severe disorder of the carboxy groups.

Versatile conformations of **TpMe** and **TpF** observed in crystalline states can be explained by the following interpretation. Namely, introduction of substituent groups into the *ortho*-positions of the carboxy group causes an increase of the rotationally variable range of the carbonyl groups, in addition to the phenylene groups. This wide range of conformations results in the generation of three polymorphs in the case of **TpMe**. However, the conformation of the **TpMe** molecule is fixed in one way in each of the polymorphs due to the bulkiness of the methyl group. In the case of **TpF**, on the other hand, the varied conformation of the peripheral groups causes no polymorphs but one crystalline form with significant disordered peripheral hydrogen-bonding groups (Fig. 4b). Probably, fluorine atoms at the *ortho*-positions are not bulky enough to affect the molecular packing and generation of polymorphs, and the varied rotational ability of the peripheral groups is neutralized by local rotational disorder.

Thermal behaviour of the frameworks

Freshly prepared crystalline bulks of **TpMe-2Ds** (which contain either one, two, or all form(s) of **TpMe-1**, **TpMe-2**, and **TpMe-3**) and **TpF-1** were subjected to thermal analysis (Fig. 5). The thermogravimetric (TG) curve of **TpMe-2Ds** revealed that the included solvent was completely released at around 200 °C. The weight loss of 38 wt% indicates that the framework involved solvent molecules (methyl benzoate) with a host–guest ratio of 1 : 4, which is also supported by ^{1}H NMR spectroscopy (Fig. S4 and S5, ESI†). The second weight loss starting from *ca.* 300 °C is assigned to thermal decomposition of the compound. **TpF-1**, the host–guest ratio of which is 1 : 7 (47 wt%) based on ^{1}H NMR spectroscopic analysis (Fig. S5, ESI†), showed ambiguous TG curves involving several steps of the weight loss. Removal of the guest molecules and thermal decomposition may occur simultaneously.

To obtain structural information during desolvation by heating, powder X-ray diffraction (PXRD) patterns of crystalline bulks of **TpMe-2Ds** and **TpF-1** were recorded with gradual heating (Fig. 6). The initial patterns are not clear, particularly in the case of **TpMe-2Ds**, due to the severe disorder of solvent molecules accommodated in voids. However, peaks gradually appeared upon heating.

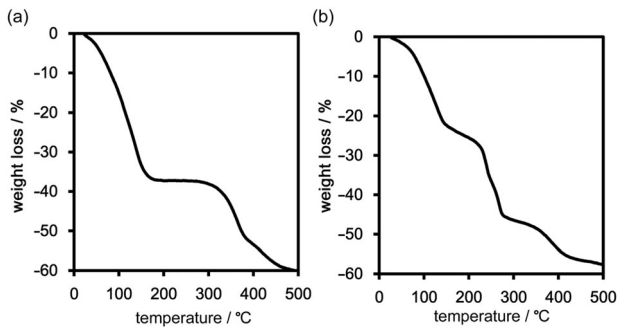

Fig. 5 TG curves of **TpMe-2Ds** and **TpF-1**.

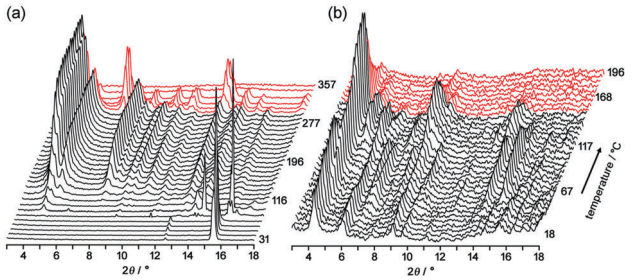

Fig. 6 Changes of PXRD patterns of (a) **TpMe-2Ds** and (b) **TpF-1** upon heating.

Upon heating of **TpMe-2Ds**, obvious peaks started to grow at 4.54°, 5.18°, 7.96° and so on at 116 °C and plateaued at around 190 °C. The obtained pattern is not in agreement with the simulated pattern of either **TpMe-1**, **TpMe-2**, or **TpMe-3**, indicating that structural changes occurred. Complete removal of the solvent molecules was confirmed by ^{1}H NMR spectroscopy. The pattern then started to change at 301 °C and completely disappeared at around 347 °C due to thermal decomposition of the compound.

In the case of **TpF-1**, the pattern change occurred in three steps, although the signal/noise ratio was relatively low. First, new peaks started to appear at around 6.9° and 7.2° at 55 °C. Then, other new peaks at 5.4° and 8.1° started to appear at 115 °C. Finally, the remaining peaks started to decay at around 155 °C and any peaks that remained disappeared at around 200 °C. This indicates that the **TpF-1** crystal changes into an amorphous phase by heating or desolvation *via* two intermediate phases. These multi-step structural changes are also implied by the TG curve (Fig. 5b).

In this way, despite the fact that both compounds have similar molecular structures and form similar LA-H-HexNets, their structure-retention ability strongly depends on the substituents at the *ortho*-positions. Particularly, it was revealed that the HexNet framework of **TpF-1** is not resistant to heat higher than *ca.* 150 °C.

Activation (desolvation with retaining pores) of **TpMe-2Ds** and **TpF-1** crystalline bulks was preliminarily attempted by heating at 100 °C or 200 °C under vacuum conditions, resulting in a significant loss of crystallinity in the case of both **TpMe-2Ds** and **TpF-1** at both temperatures. Consequently, activation was performed by a solvent exchange method. The PXRD pattern of as-formed crystalline bulks of **TpMe** again shows an ambiguous profile (Fig. 7a-ii), which is therefore difficult to be characterized when compared with the simulated pattern of **TpMe-1**, **TpMe-2**, and **TpMe-3** (Fig. 7i-1, i-2 and i-3, respectively). The as-formed crystalline bulk of **TpMe-2Ds** was soaked in benzene solution to exchange the solvent molecules in the pores. After soaking for 48 h, we confirmed by ^{1}H NMR spectroscopy that methyl benzoate was completely replaced with benzene (Fig. S6, ESI†). The resultant material showed an obvious PXRD pattern (Fig. 7a-iii). Subsequently, the materials were laid under vacuum conditions at 60 °C for 24 h, enabling complete desolvation to yield crystalline porous material **TpMe-apo** (Fig. 7a-iv and Fig. S7, ESI†).

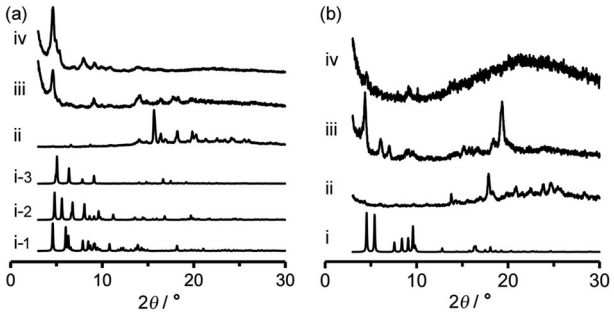

Fig. 7 PXRD pattern changes of (a) **TpMe-2Ds** and (b) **TpF-1** upon activation by a solvent exchange method. (i) Simulated PXRD patterns of **TpMe-2Ds** (i-1: **TpMe-1**, i-2: **TpMe-2**, i-3: **TpMe-3**) for (a) and **TpF-1** for (b), respectively. (ii) As-formed crystalline bulks. (iii) Benzene-soaked materials. (iv) Desolvated materials **TpMe-apo** (a) and **TpF-apo** (b).

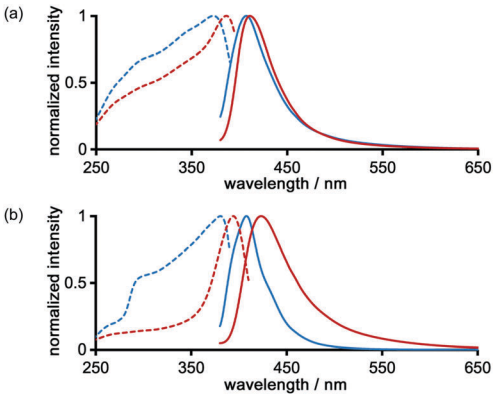

Fig. 9 Solid state excitation (dashed line) and emission (solid line) spectra of (a) **TpMe-2Ds** and (b) **TpF-1** before (blue) and after (red) desolvation [excitation wavelength (λ_{ex}) = 365 nm; detected wavelength = λ_{em}^{max}].

The PXRD pattern of **TpMe-apo** is in good agreement with that observed in VT-PXRD analysis (Fig. 6a).

Activation of **TpF-1** was performed by the same procedure as in the case of **TpMe-2Ds** except for the complete removal of benzene, which needed additional heating at 100 °C for another 24 h under vacuum conditions, to yield a desolvated material **TpF-apo** (Fig. S8–S10, ESI†). However, the crystallinity of the resultant **TpF-apo** was very low (Fig. 7b-iv).

Gas sorption properties

To evaluate the permanent porosity of **TpMe-apo** and **TpF-apo**, N_2, CO_2, and H_2 adsorption–desorption experiments were undertaken at 77 K, 195 K, and 77 K, respectively (Fig. 8). **TpMe-apo** shows a type-I sorption isotherm for all gasses, indicating that **TpMe-apo** has micropores within the framework. The amounts of uptake for N_2, CO_2, and H_2 are 182 $cm^3\ g^{-1}$, 157 $cm^3\ g^{-1}$, and 81 $cm^3\ g^{-1}$, respectively. The pore size distribution of **TpMe-apo** was calculated by the nonlocal density functional theory (NL-DFT) method (Fig. S11, ESI†), resulting in a diameter of 0.77 nm, which is in good agreement with the pore size provided by layered HexNet frameworks composed of triphenylene derivatives (**Tp-apo**). Indeed, the amounts of uptake and sorption selectively for gas species are quite similar between **TpMe-apo** and **Tp-apo**. **TpF-apo** shows quasi type-I sorption isotherms for CO_2 with an uptake of 91 $cm^3\ g^{-1}$, while it shows almost no adsorption for N_2 and H_2. This result, combined with PXRD changes upon heating, indicates that **TpF-apo** does not retain the LA-H-HexNet structure but is a less crystalline material with narrower void spaces. The surface area (SA_{BET}) calculated by the Brunauer–Emmett–Teller model for CO_2 sorption isotherms is 561 $m^2\ g^{-1}$ for **TpMe-apo** and 219 $m^2\ g^{-1}$ for **TpF-apo**. It is noteworthy that **TpF-apo** exhibits selective sorption behavior for CO_2, mainly due to the size effect of the narrow pores, and presumably due to the additional electrostatic effects of fluorine substituents, although the contribution of the latter effect is small.[25]

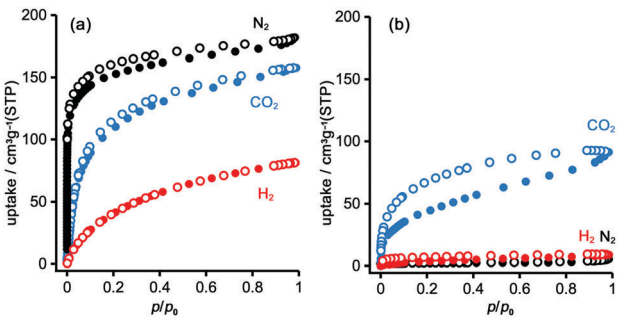

Fig. 8 Gas adsorption isotherms of (a) **TpMe-apo** and (b) **TpF-apo** for CO_2 (cyan) at 195 K, H_2 (red) at 77 K and N_2 (black) at 77 K. Solid and open symbols denote adsorption and desorption processes, respectively.

Fluorescence properties in solid states

The photochemical properties of LA-H-HexNets of **TpMe** and **TpF** were investigated before and after desolvation. Fig. 9 shows the fluorescence and excitation spectra of the as-formed crystals (**TpMe-2Ds** and **TpF-1**) and the corresponding desolvated materials (**TpMe-apo** and **TpF-apo**). **TpMe-2Ds** exhibits a structureless emission band at 407 nm (ϕ_F = 0.17, where ϕ_F denotes the fluorescence quantum yield), which was slightly red-shifted by 4 nm after desolvation (λ_{em}^{max} = 411 nm, ϕ_F = 0.09 for **TpMe-apo**). Excitation spectra are also red-shifted from 373 nm to 388 nm, indicating that intermolecular interactions between the adjacent triphenylene cores in **TpMe-apo** are stronger than those in **TpMe-2Ds**. **TpF-apo** also exhibits a structureless emission band at 423 nm (ϕ_F = 0.23), which was red-shifted by 12 nm compared with **TpF-1** (λ_{em}^{max} = 411 nm, ϕ_F = 0.16). The excitation maxima of **TpF-1** and **TpF-apo** are 381 nm and 394 nm, respectively.

Conclusions

In this paper, we synthesized two derivatives of hexakis-(carboxyphenyl)triphenylene **TpMe** and **TpF**, in which substituents (Me or F) were introduced in the *ortho*-positions of the carboxy groups, and investigated the substituent effects on the crystal structures of the LA-H-HexNets, thermal stability, and retention ability of permanent porosity. As a result, we revealed the following important features of the present system. (1) Substituent groups have no effects on the binding energy of hydrogen-bonded dimerization (~15 kcal mol^{-1}). (2) Methyl and fluorine

substituents in the *ortho*-positions of the carboxy groups made both carboxy and phenylene groups twisted, resulting in an increase of variability of peripheral conformation. (3) Depending on the bulkiness of the substituents, **TpMe** yielded three polymorphs, while **TpF** yielded one crystalline form with highly disordered peripheral groups. (4) Thermal stability and permanent porosity were drastically changed by the substituents despite the fact that both the crystals have quite similar LA-H-HexNet structures. These results can contribute to the development of functional HOFs with tunable pores based on H-HexNet frameworks.

Conflicts of interest

There are no conflicts to declare.

Acknowledgements

This work is supported by a Grant-in-Aid for Scientific Research (C) (JPT15K04591) and for Scientific Research on Innovative Areas: π-System Figuration (JP15H00998) from MEXT Japan. Synchrotron radiation experiments were undertaken at BL38B1 in SPring-8 with the approval of JASRI (proposal No. 2015B1397, 2016A1121, and 2016B1151).

Notes and references

1 G. R. Desiraju, *Angew. Chem., Int. Ed. Engl.*, 1995, **34**, 2311.
2 (*a*) G. R. Desiraju and T. Steiner, *The weak hydrogen bond*, Oxford University Press Inc., New York, 1999; (*b*) O. Ivasenko and D. F. Perepichka, *Chem. Soc. Rev.*, 2011, **40**, 191.
3 (*a*) H. Furukawa and O. M. Yaghi, *J. Am. Chem. Soc.*, 2009, **131**, 8875; (*b*) C. J. Doonan, D. J. Tranchemontagne, T. G. Glover, J. R. Hunt and O. M. Yaghi, *Nat. Chem.*, 2010, **2**, 235.
4 H. Xu, J. Gao and D. Jiang, *Nat. Chem.*, 2015, **7**, 905.
5 (*a*) G. Das, B. P. Biswal, S. Kandambeth, V. Venkatesh, G. Kaur, M. Addicoat, T. Heine, S. Verma and R. Banerjee, *Chem. Sci.*, 2015, **6**, 3931; (*b*) Z. Li, Y. Zhang, H. Xia, Y. Mu and X. Liu, *Chem. Commun.*, 2016, **52**, 6613; (*c*) N. Huang, X. Ding, J. Kim, H. Ihee and D. Jiang, *Angew. Chem., Int. Ed.*, 2015, **54**, 8704; (*d*) Y. Peng, Y. Huang, Y. Zhu, B. Chen, L. Wang, Z. Lai, Z. Zhang, M. Zhao, C. Tan, N. Yang, F. Shao, Y. Han and H. Zhang, *J. Am. Chem. Soc.*, 2017, **139**, 8698; S.-Y. Ding, M. Dong, Y.-W. Wang, Y.-T. Chen, H.-Z. Wang, C.-Y. Su and W. Wang, *J. Am. Chem. Soc.*, 2016, **138**, 3031.
6 (*a*) T. Kambe, R. Sakamoto, T. Kusamoto, T. Pal, N. Fukui, K. Hoshiko, T. Shimojima, Z. Wang, T. Hirahara, K. Ishizaka, S. Hasegawa, F. Liu and H. Nishihara, *J. Am. Chem. Soc.*, 2014, **136**, 14357; (*b*) J. Guo., Y. Xu, S. Jin, L. Chen, T. Kaji, Y. Honsho, M. A. Addicoat, J. Kim, A. Saeki, H. Ihee, S. Seki, S. Irle, M. Hiramono, J. Gao and D. Jiang, *Nat. Commun.*, 2013, **4**, 2736; (*c*) M. Dogru, M. Handloser, F. Auras, T. Kunz, D. Medina, A. Hartschuh, P. Knochel and T. Bein, *Angew. Chem., Int. Ed.*, 2013, **52**, 2920; (*d*) M. Calik, F. Auras, L. M. Salonen, K. Bader, I. Grill, M. Handloser, D. D. Medina, M. Dogru, F. Löbermann, D. Trauner, A. Hartschuh and T. Bein, *J. Am. Chem. Soc.*, 2014, **136**, 17802.
7 M. Zhao, Q. Lu, Q. Ma and H. Zhang, *Small Methods*, 2017, **1**, 1600030.
8 (*a*) X. Feng, X. Ding and D. Jiang, *Chem. Soc. Rev.*, 2012, **41**, 6010; (*b*) S.-Y. Ding and W. Wang, *Chem. Soc. Rev.*, 2013, **42**, 548; (*c*) N. Huang, P. Wang and D. Jiang, *Nat. Rev. Mater.*, 2016, **1**, 16068.
9 (*a*) J. Lu and R. Cao, *Angew. Chem., Int. Ed.*, 2016, **55**, 9474; (*b*) A. R. A. Palmans, J. A. J. M. Vekemans, H. Kooijman, A. L. Spek and E. W. Meijer, *Chem. Commun.*, 1997, 2247; (*c*) P. Sozani, S. Bracco, A. Comotti, L. Ferretti and R. Simonutti, *Angew. Chem., Int. Ed.*, 2005, **44**, 1816; (*d*) X.-Z. Luo, X.-J. Jia, J.-H. Deng, J.-L. Zhong, H.-J. Liu, K.-J. Wang and D.-C. Zhong, *J. Am. Chem. Soc.*, 2013, **135**, 11684; (*e*) T.-H. Chen, I. Popov, W. Kaveevivitchai, Y.-C. Chuang, Y.-S. Chen, O. Daugulis, A. J. Jacobson and O. Š. Miljanić, *Nat. Commun.*, 2014, **5**, 5131; (*f*) P. Li, Y. He, Y. Zhao, L. Weng, H. Wang, R. Krishna, H. Wu, W. Zhou, M. O'Keeffe, Y. Han and B. Chen, *Angew. Chem., Int. Ed.*, 2015, **54**, 574.
10 (*a*) D. J. Duchamp and R. Marsh, *Acta Crystallogr., Sect. B: Struct. Crystallogr. Cryst. Chem.*, 1969, **25**, 5; (*b*) F. H. Herbstein, M. Kapon and G. M. Reisner, *J. Inclusion Phenom.*, 1987, **5**, 211; (*c*) K. Kobayashi, T. Shirasaka, E. Horn and N. Furukawa, *Tetrahedron Lett.*, 2000, **41**, 89; (*d*) I. Hisaki, N. Q. E. Affendy and N. Tohnai, *CrystEngComm*, 2017, **19**, 4892.
11 (*a*) C. A. Zentner, H. W. H. Lai, J. T. Greenfield, R. A. Wiscons, M. Zeller, C. F. Campana, O. Talu, S. A. FitzGerald and J. L. C. Rowsell, *Chem. Commun.*, 2015, **51**, 11642; (*b*) S. Nandi, D. Chakraborty and R. Vaidhyanathan, *Chem. Commun.*, 2016, **52**, 7249; (*c*) F. Hu, C. Liu, M. Wu, J. Pang, F. Jiang, D. Yuan and M. Hong, *Angew. Chem., Int. Ed.*, 2017, **56**, 2101; (*d*) I. Hisaki, N. Ikenaka, E. Gomez, B. Cohen, N. Tohnai and A. Douhal, *Chem. – Eur. J.*, 2017, **23**, 11611.
12 (*a*) I. Hisaki, S. Nakagawa, N. Tohnai and M. Miyata, *Angew. Chem., Int. Ed.*, 2015, **54**, 3008; (*b*) I. Hisaki, N. Ikenaka, N. Tohnai and M. Miyata, *Chem. Commun.*, 2016, **52**, 300; (*c*) I. Hisaki, S. Nakagawa, N. Ikenaka, Y. Imamura, M. Katouda, M. Tashiro, H. Tsuchida, T. Ogoshi, H. Sato, N. Tohnai and M. Miyata, *J. Am. Chem. Soc.*, 2016, **138**, 6617; (*d*) I. Hisaki, S. Nakagawa, H. Sato and N. Tohnai, *Chem. Commun.*, 2016, **52**, 9781; (*e*) I. Hisaki, H. Toda, H. Sato, N. Tohnai and H. Sakurai, *Angew. Chem., Int. Ed.*, 2017, **56**, 15294.
13 (*a*) M. Mastalerz and I. Oppel, *Angew. Chem., Int. Ed.*, 2012, **51**, 5252; (*b*) W. Yan, X. Yu, T. Yan, D. Wu, E. Ning, Y. Qi, Y.-F. Han and Q. Li, *Chem. Commun.*, 2017, **53**, 366.
14 (*a*) B. Ośmiałowsky, E. Kolehmainen, R. Gawinecki, R. Dobosz and R. Kauppinen, *J. Phys. Chem. A*, 2010, **114**, 12881–12887; (*b*) B. Ośmiałowsky, E. Kolehmainen and M. Kowalska, *J. Org. Chem.*, 2012, **77**, 1653.
15 B. Ośmiałowsky, E. Kolehmainen, R. Gawinecki, R. Kauppinen, J. Koivukorpi and A. Valkonen, *Struct. Chem.*, 2010, **21**, 1061.
16 Rigaku Oxford Diffraction (2015), Software CrysAlisPro 1.171.38.41o, Rigaku Corporation, Tokyo, Japan.

17 HKL2000. Z. Otwinowski and W. Minor, *Methods Enzymol.*, 1997, **276**, 307.
18 G. M. Sheldrick, *Acta Crystallogr., Sect. A: Found. Adv.*, 2015, **71**, 3.
19 Rigaku (2015), CrystalStructure. Ver. 4.2, Rigaku Corporation, Tokyo, Japan.
20 G. M. Sheldrick, *Acta Crystallogr., Sect. C: Struct. Chem.*, 2015, **71**, 3.
21 (*a*) P. v. d. Sluis and A. L. Spek, *Acta Crystallogr., Sect. A: Found. Crystallogr.*, 1990, **46**, 194; (*b*) A. L. Spek, *Acta Crystallogr., Sect. D: Biol. Crystallogr.*, 2009, **65**, 148.
22 M. J. Frisch, G. W. Trucks, H. B. Schlegel, G. E. Scuseria, M. A. Robb, J. R. Cheeseman, G. Scalmani, V. Barone, B. Mennucci, G. A. Petersson, H. Nakatsuji, M. Caricato, X. Li, H. P. Hratchian, A. F. Izmaylov, J. Bloino, G. Zheng, J. L. Sonnenberg, M. Hada, M. Ehara, K. Toyota, R. Fukuda, J. Hasegawa, M. Ishida, T. Nakajima, Y. Honda, O. Kitao, H. Nakai, T. Vreven, J. A. Montgomery, Jr., J. E. Peralta, F. Ogliaro, M. Bearpark, J. J. Heyd, E. Brothers, K. N. Kudin, V. N. Staroverov, R. Kobayashi, J. Normand, K. Raghavachari, A. Rendell, J. C. Burant, S. S. Iyengar, J. Tomasi, M. Cossi, N. Rega, J. M. Millam, M. Klene, J. E. Knox, J. B. Cross, V. Bakken, C. Adamo, J. Jaramillo, R. Gomperts, R. E. Stratmann, O. Yazyev, A. J. Austin, R. Cammi, C. Pomelli, J. W. Ochterski, R. L. Martin, K. Morokuma, V. G. Zakrzewski, G. A. Voth, P. Salvador, J. J. Dannenberg, S. Dapprich, A. D. Daniels, Ö. Farkas, J. B. Foresman, J. V. Ortiz, J. Cioslowski and D. J. Fox, *Gaussian 09, Revision C.01*, Gaussian, Inc., Wallingford CT, 2009.
23 B. J. Ransil, *J. Chem. Phys.*, 1961, **34**, 2109.
24 S. F. Boys and F. Bernardi, *Mol. Phys.*, 1970, **19**, 553.
25 A. Torrisi, C. Mellot-Draznieks and R. G. Bell, *J. Chem. Phys.*, 2009, **130**, 194703.

